Spin dynamics of excited trion states in a single InAs quantum dot

Y. Igarashi,[1,2,*] M. Shirane,[1,2] Y. Ota,[2,3] M. Nomura,[2] N. Kumagai,[2] S. Ohkouchi,[2] A. Kirihara,[1,2] S. Ishida,[2,3] S. Iwamoto,[2,3] S. Yorozu,[1,2] and Y. Arakawa[2,3]

[1]*Green Innovation Research Laboratories, NEC Corporation, 34 Miyukigaoka, Tsukuba-shi, Ibaraki 305-8501, Japan*

[2]*Institute for Nano Quantum Information Electronics, The University of Tokyo, 4-6-1 Komaba, Meguro-ku, Tokyo 153-8505, Japan*

[3]*Institute of Industrial Science, The University of Tokyo, 4-6-1 Komaba, Meguro-ku, Tokyo 153-8505, Japan*

(Received 14 May 2010; published 4 June 2010)

We measure photon cross-correlation between two positively charged biexcitonic emission lines and a positively charged excitonic line for a single InAs/GaAs quantum dot (QD). Marked difference in the correlation function is observed, which originates from multiple spin configurations of intermediate states, i.e., excited positively charged exciton (trion) states. With the aid of a rate equation simulation, we evaluate the transition rate with *p*-shell hole-spin flip to be 0.8–1.0 GHz, which is almost comparable to the radiative decay rate of the ground charged exciton, presumably due to the spin scattering between carriers in a QD and a wetting layer and/or mixing of the excited trion states. In contrast, the relaxation rate with conserving *p*-shell hole-spin projection is estimated to be about one order of magnitude higher than that with hole-spin flip.

DOI: 10.1103/PhysRevB.81.245304 PACS number(s): 78.55.Cr, 71.35.Pq, 71.70.Gm, 78.67.Hc

I. INTRODUCTION

Strong quantum confinement of a semiconductor quantum dot (QD) exhibits peculiar and different characteristics from bulk material, such as atomlike discrete energy dispersion of carriers. In that sense, QDs can provide an ideal platform to perform fundamental research on quantum optics and quantum electronics, which otherwise can barely be explored. Moreover, the long coherence time of spins in a QD is attractive for applying to the spin-based quantum information devices. The charged exciton (trion) in a QD holds an unpaired electron or hole spin, which can be optically excited and detected,[1,2] and is one of the conceivable candidates for realizing the spin memory[3,4] or spin state quantum computing.[5–7] For those reasons, interest is growing in the QD trion both theoretically and experimentally. The negative ground trion, which is composed of one hole and two electrons in the *s*-shell ($1e^2 1h^1$), has been relatively well examined and understood (e.g., Ref. 2). However, there have only been several reports on excited negative trions,[8–13] and even fewer on excited positive trions.[14–16] The excited trions consist of an electron-hole (e-h) pair in the *s* shell and an electron or a hole in higher shells with various spin configurations. This leads to complicated fine structures of the excited trion states, which arise from exchange interaction. Nevertheless, there has been little study done on the carrier dynamics of the excited trion states on the basis of the spin configuration, though it is both of sincere interest for fundamental physics and of great importance for the device application. Photon correlation measurement is one of the most powerful experimental methods that enable us to study such carrier dynamics in QDs. The discussion can apply to other spin-related physical systems, which are optically detected or controlled.

We examined the positively charged biexcitonic state (XX^+), which consists of two e-h pairs in the *s* shell and a hole in the *p* shell ($1e^2 1h^2 2h^1$), in a self-assembled InAs/GaAs QD by using photoluminescence (PL) and photon correlation measurements. One of the *s*-shell e-h pairs in XX^+ recombines with optical radiation, leaving behind the excited positive trion state (X^{+*}), which is composed of an e-h pair in the *s*-shell and a remnant hole in the *p*-shell ($1e^1 1h^1 2h^1$). Due to the e-h and hole-hole (h-h) exchange interaction, X^{+*} states have four doubly degenerate branches. In this study, we identified PL peaks corresponding to those X^{+*} states and evaluated the different carrier-relaxation rates from X^{+*} states to the ground trion (X^+) state in accordance with the different spin configurations by comparing the photon correlation measurements with numerical simulations.

II. EXPERIMENTAL

The sample under investigation was grown by molecular beam epitaxy on a (001) GaAs substrate. A single InAs QD layer was capped with an 80-nm-thick GaAs layer. The estimated areal density of the QDs was $\sim 5 \times 10^9$ cm^{-2}, and the recombination energy for a typical QD was tuned to around 1.28–1.35 eV at 10 K by using an In-flush technique.[17] The details of the growth conditions can be found elsewhere.[18] To excite only a single or a few QD(s), we fabricated 0.4-μm-diameter mesa structures by electron beam lithography and inductively coupled plasma reactive ion etching.

Our experiments were performed at cryogenic temperature using a μ-PL setup. The sample was excited by a continuous wave Ti:sapphire laser operated at 1.55 eV (above-band excitation). The excitation beam was focused on the sample to a spot size of ~ 3 μm with the microscopic objective lens ($\times 40$, NA=0.60). The PL was collected by the same lens and spectrally analyzed by a grating monochromator equipped with liquid-nitrogen-cooled Si charge-coupled device arrays. In addition, photon cross-correlation measurements were performed by using a Hanbury Brown-Twiss (HBT) setup.[19] A pair of Si avalanche photodiodes (APDs) located behind the monochromators, whereby the PL spectrum within an energy window of 0.36 meV was extracted, was incorporated to record histograms of coincidence counts for photon arrivals at both APDs.

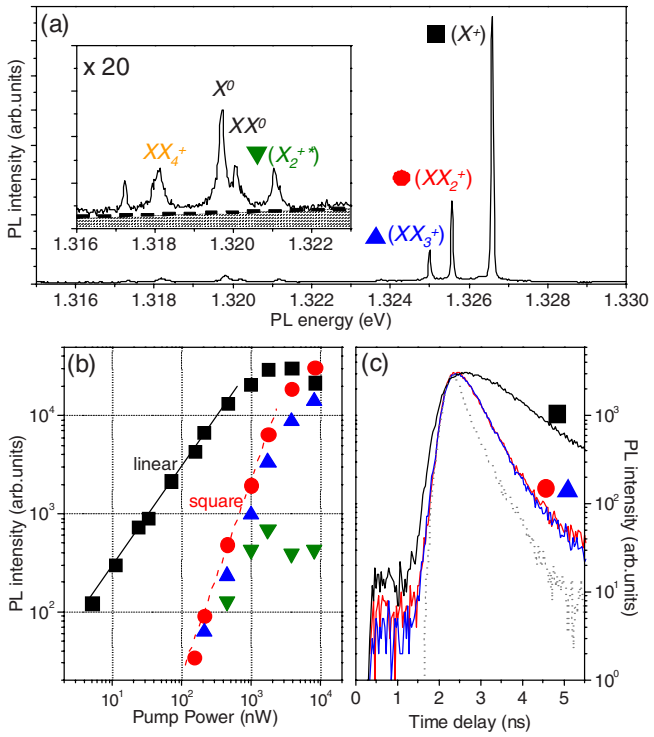

FIG. 1. (Color online) (a) Observed PL spectrum at $P=1.74$ μW. Inset shows the PL spectrum magnified by a factor 20. The shaded region indicates a background emission, which is properly subtracted when analyzing the data. (b) Pump power dependence of the observed PL peaks. The experimental data plotted by black squares etc. correspond to the PL lines labeled by the same symbols in (a). The solid (dashed) line is a guide of linear (square) power dependence. (c) The time resolved PL intensities for the (bi)excitonic peaks measured under a mode-locked pulse excitation (80 MHz repetition, 2 ps pulse duration). The system response measured by scattered incident laser beam is shown as gray dashed curve for comparison.

III. RESULTS AND DISCUSSIONS

Figure 1(a) shows the μ-PL spectrum of a single QD for a pump power (defined as the power at the sample surface) $P=1.74$ μW. A distinct peak labeled by a square, followed by two peaks labeled by a circle and an upward triangle, is clearly seen within a spectral window of interest. As is shown in Fig. 1(b), PL intensity of the square increases linearly with P, while those of the circle and the upward triangle increase quadratically. This indicates the (bi)excitonic characteristics of the PL peak(s) represented by the square (circle and upward triangle). Figure 1(c) shows the observed time resolved PL intensities. The estimated decay constant for the square ($\tau_X=1.25$ ns) is roughly twice as long as that for both the circle and upward triangle ($\tau_{XX}=0.51$ ns). That decay constants estimated for the two biexcitonic PL peaks are exactly the same suggests that the initial state (XX^+) for the two peaks was identical. Considering this and also other experimental evidences, we attribute the excitonic PL peak (square) to the radiative decay from X^+ state and biexcitonic peaks (circle and upward triangle) to those from XX^+ state to X^{+*} states ($1e^21h^22h^1 \rightarrow 1e^11h^12h^1$).

Because the X^{+*} consists of an e-h pair in the s-shell and a hole in the p-shell, there are $2^3=8$ possible spin configurations, which naively leads to the eightfold degeneracy. Taking into account the h-h and e-h exchange interaction, the eightfold degeneracy of X^{+*} is lifted to four degenerate doublets. One of the branches, "singlet state," is named after the fact the two holes in the s- and p-shell compose a spin singlet, where the total spin z-projection of the composite is $m_z=\pm 1/2$. In a similar fashion, the others are named "triplet states," the total spin z-projections of which are $m_z=\pm 1/2, \pm 5/2, \pm 7/2$. Total energy of the singlet state is generally higher than the triplet states due to the isotropic h-h exchange interaction being much larger than the e-h exchange interaction.[20] (We label X_4^{+*} for the singlet state.) In contrast, total energy of the triplet state with $m_z=\pm 7/2$ (labeled X_1^{+*}) is the lowest in energy due to the largest e-h exchange interaction for this case. However, the energy relationship between the other two triplet branches with $m_z=\pm 1/2$ (labeled X_3^{+*}) and $\pm 5/2$ (labeled X_2^{+*}) is not so straightforward. According to Fermi's golden rule, a transition matrix element of $XX^+ \rightarrow X_2^{+*}$ should be twice as large as that of $XX^+ \rightarrow X_3^{+*}$ due to the corresponding spin configurations.[10,11] Looking carefully at Fig. 1(b), the peak intensity of one of the biexcitonic emission lines represented by the circle stays almost twice as large as the other biexcitonic line represented by the upward triangle until saturation, thus we identify that the PL peak represented by the circle (upward triangle) corresponds to the radiative decay from $XX^+ \rightarrow X_2^{+*}$ (X_3^{+*}). Hereafter, we abbreviate the emission line of $XX^+ \rightarrow X_i^{+*}$ as XX_i^+ for simplicity and rename the biexcitonic line represented by the circle (upward triangle) as $XX_{2(3)}^+$.

We also identify the XX_4^{+*} PL line. Without changing the spin states, the X_4^{+*} state can quickly relax into X^+ state, approximately on the time scale of ps.[11] This short lifetime of the final state leads to the broadening of the XX_4^{+*} PL peak due to the time-energy uncertainty relationship.[21] The same applies to the PL line for $X_2^{+*} \rightarrow 0^{+*}$ (labeled X_2^{+*} for simplicity), where 0^{+*} is an excited hole-spin state ($1h^02h^1$). Inset of Fig. 1(a) shows a magnified PL spectrum at the same pump power. The peaks preliminarily labeled "XX_4^+" and "X_2^{+*}" are obviously broad with full width at half maximum (FWHM) in the range of 0.2–0.3 meV. Taking into account the numerically simulated (explained later) pump power dependence of these PL peaks, we identify that the broad peak at 1.318 (1.321) eV corresponds to XX_4^+ (X_2^{+*}). The energy separation between X_4^{+*} singlet state and X_2^{+*} triplet state is estimated to be 7.3 meV, which is a typical value for an InAs QD of almost the same size.[15] Owing to the pump power dependence, a neutral (bi)excitonic peak X^0 (XX^0) are also identified (see Fig. 1(a) inset).

On the basis of the discussion above, Fig. 2 shows the schematic energy diagram for XX^+ and $X^{+(*)}$ states. Here, a single-line-arrow $\uparrow(\downarrow)$ depicts an s-shell electron with $m_z=+1/2(-1/2)$, and a double-line-arrow $\Uparrow(\Downarrow)$ depicts an s-shell heavy hole with $m_z=+3/2(-3/2)$. In a very similar way, a large double-line-arrow represents a p-shell heavy hole. Normalization factors are omitted, and one of the possible spin configurations is presented for convenience. The X_1^{+*} state with $m_z=\pm 7/2$ is schematized as a dotted line

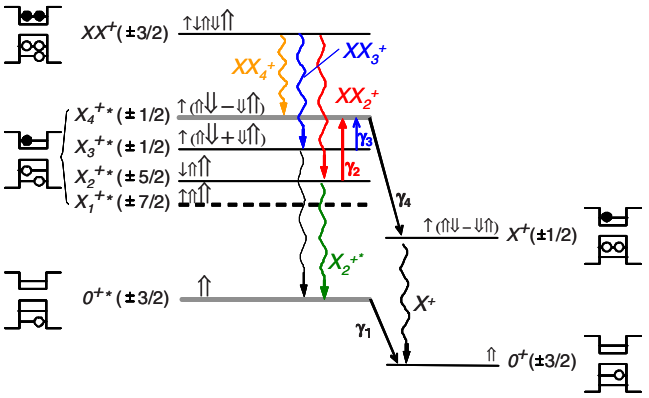

FIG. 2. (Color online) Schematic energy diagram of positively charged biexcition and excited (ground) positive trion states. One of the possible spin configurations is shown for each level, where $\uparrow(\Uparrow)$ depicts an *s*-shell electron (hole) and a large $\Uparrow$ depicts a *p*-shell hole. The wavy arrows denote the radiative decays, while the linear arrows labeled γ_i denote the nonradiative transitions.

because the transition from XX^+ state to X_1^{+*} state is optically forbidden by the spin selection rule.

To further verify this energy diagram and investigate the carrier dynamics between X_i^{+*} states and X^+ state, we performed the photon cross-correlation measurements using the HBT setup. The Poisson-normalized second-order correlation function

$$g^{(2)}(\tau) = \langle I_1(t) I_2(t+\tau)\rangle / \langle I_1(t)\rangle\langle I_2(t)\rangle,$$

experimentally obtained for $XX^+_{3(2)}$-X^+ is plotted in Fig. 3(a) [Fig. 3(b)], where $\langle I_j(t)\rangle$ is a statistical average of the photon counts detected at APD_j and τ is a time delay between APD_1 and APD_2, using the $XX^+_{3(2)}$ emission line as the "start" and the $X^+ \rightarrow 0^+$ emission line as the "stop." The peak (dip) structure in $g^{(2)}(\tau)$ is called (anti-)bunching, which means the enhancement (suppression) of multiphoton detection probability. The temporal resolution of our system was 700 ps (FWHM), leading to rather smooth (anti-)bunching structures. In Fig. 3(a), the bunching behavior clearly seen for XX_3^+-X^+ at $\tau > 0$, accompanied with the antibunching behavior for $\tau < 0$, indicates the indirect cascade radiation of XX_3^+ to X^+. Therefore, the carrier relaxation rate from intermediate X_3^{+*} state (via X_4^{+*} state) to X^+ state must be higher than Γ_X, the radiative decay rate of X^+. Meanwhile, no bunching behavior is observed for XX_2^+-X^+ at $\tau > 0$. This indicates that the carrier relaxation rate from X_2^{+*} state (via X_4^{+*} state) to X^+ state is lower than or at most comparable to Γ_X. For this reason, the $X_2^{+*} \rightarrow 0^{+*}$ radiative decay before relaxing into X^+ state can be observed in Fig. 1(a) inset, as was observed previously for an excited negative trion[8] and recently for an excited positive trion.[15,16] The origin of this different behaviors in Figs. 3(a) and 3(b) can be understood as follows. For XX_3^+-X^+, the total spin z projection $m_z = \pm 1/2$ of X_3^{+*} state is the same as the singlet state X_4^{+*}. It needs only relative phase π-shift for spin configuration to be primarily excited to X_4^{+*} and subsequently relax into X^+ state. On the other hand, spin z projection is not conserved for $X_2^{+*} \rightarrow X_4^{+*}$, therefore the rate of which becomes much lower than the case before.

To verify the speculation above, photon cross-correlation functions were numerically simulated by using a rate equation considering all the levels shown in Fig. 2. The photon emission from the other unidentified background oscillators[22] and also the finite time resolution of the system[23] are considered in our calculations. A charged triexciton level (not shown in Fig. 2) is practically included so that the population of the XX^+ state would not artificially saturate at a high pump rate region.[24] Events of both e-h pair creation and an independent single electron or hole capturing are also included to

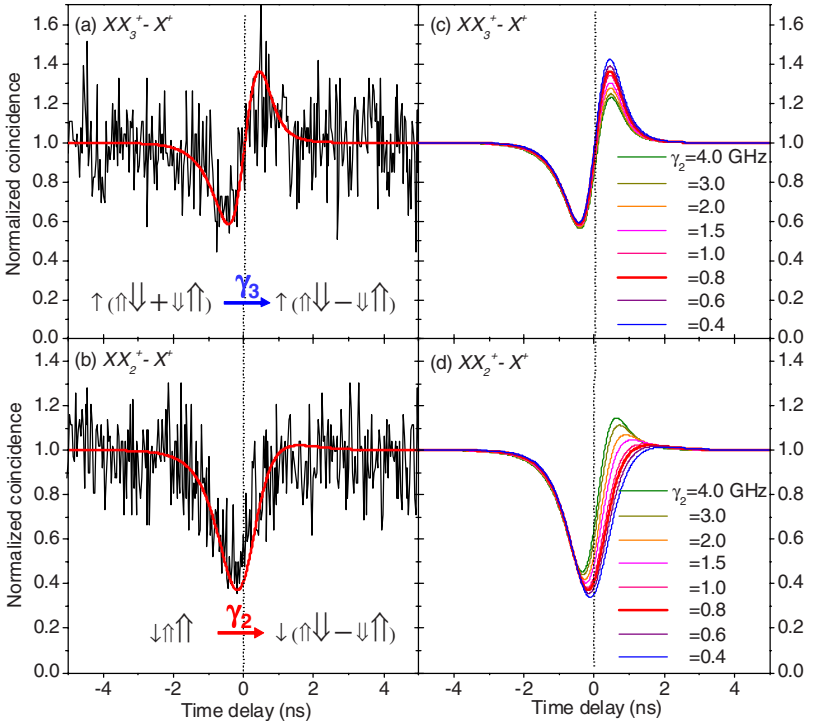

FIG. 3. (Color online) Normalized cross-correlation function for XX_3^+-X^+ (a) and for XX_2^+-X^+ (b). The red lines are the best matching simulation results, where $\gamma_2 = 0.8$ GHz and $\gamma_3 = 10\Gamma_X$. The numerically simulated $g^{(2)}(\tau)$ for XX_3^{+*}-X^+ and XX_2^{+*}-X^+ are shown in (c) and (d) for various value of γ_2 from 0.4 to 4.0 GHz.

represent the above-band excitation.[25] The radiative decay rate Γ_X and Γ_{XX} are extracted from our experiment, where $\Gamma_X = 1/\tau_X$, $\Gamma_{XX} = 1/\tau_{XX}$. As previously explained, the PL peak of $X_2^{+*}(XX_4^+)$ is substantially broad (FWHM of 0.2–0.3 meV) due to the high relaxation-rate $\gamma_{1(4)}$ of the final state $0^{+*}(X_4^{+*})$, which leads to an upper limit of $\gamma_1, \gamma_4 < 300$ GHz. On the contrary, the linewidth of X^+ PL peak (~ 60 μeV) is restricted by energy resolution and spectral diffusion. This leads to a lower limit of ~ 100 GHz for γ_1 and γ_4. Hence, $\gamma_1 = \gamma_4$ of 200 GHz are assumed in our calculation. These high $p \rightarrow s$ energy relaxation rates can be attributed to emission of a resonant LA phonon with less than few meV energy, where the phonon wavelength can exceed the corresponding QD diameter.[26] Meanwhile, the resolution limited linewidth of X^+ also provides an upper limit of 100 GHz for the transition rates $\gamma_{2(3)}$ from $X_{2(3)}^{+*}$ states to X_4^{+*} state. We found that γ_2 is a key parameter, which determines the behavior of the correlation function $g^{(2)}(\tau)$, and that γ_3 least affects $g^{(2)}(\tau)$ within its reasonable range. The solid red curves in Figs. 3(a) and 3(b) are the best fitting ones simulated, where γ_3/Γ_X is set to 10. (Note that in Fig. 1(a) inset the $X_3^{+*} \rightarrow 0^{+*}$ radiative decay line should have been observed at 1.3216 eV owing to the energy diagram shown in Fig. 2 if γ_3 were as low as γ_2 or Γ_X.) The simulation agrees well with our experimental results. Figure 3(c) [Fig. 3(d)] shows calculated γ_2 dependence of $g^{(2)}(\tau)$ for $XX_{3(2)}^{+*}$-X^+. For XX_3^{+*}-X^+, the smaller the γ_2, the higher bunching $g^{(2)}(\tau)$ at $\tau > 0$. In contrast, $g^{(2)}(\tau)$ for XX_2^{+*}-X^+ exhibits the opposite behavior. The $g^{(2)}(\tau) > 1$ for the highest γ_2 gradually decreases as γ_2 decreases, and eventually for $\gamma_2 < 1$ GHz the bunching structure is lost and $g^{(2)}(\tau)$ becomes smaller than 1 (antibunching). Comparing the experimental results and simulations for $XX_{2(3)}^{+*}$-X^+, we deduce the γ_2 to be lower than 1.0 GHz.

However, suppose $\gamma_2 < \Gamma_X = 0.8$ GHz, PL intensity for X_2^{+*} should be more than a half the PL intensity for XX_2^{+*} at a relatively low-pump power region. This is not the case for the experimental results, like in Fig. 1(b), where the PL intensity for X_2^{+*} does not exceed half that for XX_2^{+*}. This provides the lower limit for γ_2, therefore $\gamma_2 = 0.8-1.0$ GHz is deduced to fulfill the above competitive requirements.

The estimated γ_2 is higher than that under quasiresonant excitation for X^{-*}.[8] One of the possible mechanism for this high transition-rate is a spin-flip process between carriers in a QD and excess carriers in the wetting layer, as we excite the above band of GaAs. This is not quite surprising as there has been an experimental report on the broadening of a QD PL peak due to the scattering arising within the tail of continuum states.[27] A theoretical report also suggests that the absorption peak exists near the continuum state.[28] Another possible reason for the high γ_2 rate is the mixing of triplet X_2^{+*} state and X_3^{+*} state due to the anisotropic e-h exchange interaction, which is described as follows:[20]

$$|X_2^{+*}\rangle = \cos\alpha \left|\pm\frac{5}{2}\right\rangle - \sin\alpha \left|\mp\frac{1}{2}\right\rangle,$$

$$|X_3^{+*}\rangle = \cos\alpha \left|\pm\frac{1}{2}\right\rangle + \sin\alpha \left|\mp\frac{5}{2}\right\rangle.$$

We performed the polarization measurement for XX_i^+ and deduced the amount of wave function mixing $\alpha = 0.23$, which means $\simeq 5\%(=\sin^2\alpha)$ mixing. Therefore, the experimentally estimated γ_2 can be also attributed to the mixed X_3^{+*} wave function component, the intrinsic transition rate of which to X_4^{+*} is much higher than that for X_2^{+*}.

IV. CONCLUSION

We measured the radiative decays from XX^+ and X^+ states. The intermediate X^{+*} states consists of a hole-spin singlet state and three degeneracy-lifted hole-spin triplet states. We identified three optically allowed transitions from XX^+ states, namely, XX_2^+, XX_3^+, and XX_4^+. Different spin configurations of these X^{+*} states lead to the different relaxation rates to X^+ state. We measured the photon cross-correlation functions for $XX_{2(3)}^+ - X^+$ and found significant difference between them. By comparing the experiments with the numerical simulations based on the stochastic rate equation method, we quantitatively evaluate the relaxation rate γ_2 of 0.8-1.0 GHz with p-shell hole-spin flip. The relaxation rate γ_3 with relative phase shift is estimated to be about at least one order of magnitude higher than γ_2, without the need for p-shell hole-spin flip.

ACKNOWLEDGMENTS

We thank S. Kono and K. Watanabe for their technical support. This work was performed by the Special Coordination Funds for Promoting Science and Technology, Japan Science and Technology Agency.

*y-igarashi@bp.jp.nec.com

[1] S. Cortez, O. Krebs, S. Laurent, M. Senes, X. Marie, P. Voisin, R. Ferreira, G. Bastard, J.-M. Gérard, and T. Amand, Phys. Rev. Lett. **89**, 207401 (2002).

[2] D. Press, T. D. Ladd, B. Zhang, and Y. Yamamoto, Nature (London) **456**, 218 (2008).

[3] M. Kroutvar, Y. Ducommun, D. Heiss, M. Bichler, D. Schuh, G. Abstreiter, and J. J. Finley, Nature (London) **432**, 81 (2004).

[4] D. Brunner, B. D. Gerardot, P. A. Dalgarno, G. Wüst, K. Karrai, N. G. Stoltz, P. M. Petroff, and R. J. Warburton, Science **325**, 70 (2009).

[5] A. Imamoglu, D. D. Awschalom, G. Burkard, D. P. DiVincenzo, D. Loss, M. Sherwin, and A. Small, Phys. Rev. Lett. **83**, 4204 (1999).

[6] X. Xu, Y. Wu, B. Sun, Q. Huang, J. Cheng, D. G. Steel, A. S. Bracker, D. Gammon, C. Emary, and L. J. Sham, Phys. Rev. Lett. **99**, 097401 (2007).

[7] M. Atatüre, J. Dreiser, A. Badolato, A. Högele, K. Karrai, and A. Imamoglu, Science **312**, 551 (2006).

[8] S. M. Ulrich, M. Benyoucef, P. Michler, N. Baer, P. Gartner, F.

Jahnke, M. Schwab, H. Kurtze, M. Bayer, S. Fafard, Z. Wasilewski, and A. Forchel, Phys. Rev. B **71**, 235328 (2005).
[9] I. A. Akimov, A. Hundt, T. Flissikowski, and F. Henneberger, Appl. Phys. Lett. **81**, 4730 (2002).
[10] I. A. Akimov, K. V. Kavokin, A. Hundt, and F. Henneberger, Phys. Rev. B **71**, 075326 (2005).
[11] M. E. Ware, E. A. Stinaff, D. Gammon, M. F. Doty, A. S. Bracker, D. Gershoni, V. L. Korenev, Ş. C. Bădescu, Y. Lyanda-Geller, and T. L. Reinecke, Phys. Rev. Lett. **95**, 177403 (2005).
[12] I. E. Kozin, V. G. Davydov, I. V. Ignatiev, A. V. Kavokin, K. V. Kavokin, G. Malpuech, Hong-Wen Ren, M. Sugisaki, S. Sugou, and Y. Masumoto, Phys. Rev. B **65**, 241312(R) (2002).
[13] H. Sanada, T. Sogawa, H. Gotoh, Y. Tokura, H. Yamaguchi, H. Nakano, and H. Kamada, Phys. Rev. B **79**, 121303(R) (2009).
[14] R. Seguin, S. Rodt, A. Schliwa, K. Pötschke, U. W. Pohl, and D. Bimberg, Phys. Status Solidi B **243**, 3937 (2006).
[15] T. Warming, E. Siebert, A. Schliwa, E. Stock, R. Zimmermann, and D. Bimberg, Phys. Rev. B **79**, 125316 (2009).
[16] E. Poem, Y. Kodriano, C. Tradonsky, B. D. Gerardot, P. M. Petroff, and D. Gershoni, Phys. Rev. B **81**, 085306 (2010).
[17] Z. R. Wasilewski, S. Fafard, and J. P. McCaffrey, J. Cryst. Growth **201-202**, 1131 (1999).
[18] N. Kumagai, S. Ohkouchi, S. Nakagawa, M. Nomura, Y. Ota, M. Shirane, Y. Igarashi, S. Yorozu, S. Iwamoto, and Y. Arakawa, Physica E (Amsterdam) (to be published).
[19] R. Hanbury Brown and R. Q. Twiss, Nature (London) **177**, 27 (1956).
[20] K. V. Kavokin, Phys. Status Solidi A **195**, 592 (2003).
[21] R. J. Warburton, C. Schäflein, D. Haft, F. Bickel, A. Lorke, K. Karrai, J. M. Garcia, W. Schoenfeld, and P. M. Petroff, Nature (London) **405**, 926 (2000).
[22] R. Brouri, A. Beveratos, J. P. Poizat, and P. Grangier, Opt. Lett. **25**, 1294 (2000).
[23] S. M. Ulrich, C. Gies, S. Ates, J. Wiersig, S. Reitzenstein, C. Hofmann, A. Löffler, A. Forchel, F. Jahnke, and P. Michler, Phys. Rev. Lett. **98**, 043906 (2007).
[24] G. Sallen, A. Tribu, T. Aichele, R. André, L. Besombes, C. Bougerol, S. Tatarenko, K. Kheng, and J. Ph. Poizat, Phys. Rev. B **80**, 085310 (2009).
[25] C. Santori, D. Fattal, J. Vučković, G. S. Solomon, E. Waks, and Y. Yamamoto, Phys. Rev. B **69**, 205324 (2004).
[26] U. Bockelmann and G. Bastard, Phys. Rev. B **42**, 8947 (1990).
[27] B. Urbaszek, E. J. McGhee, M. Krüger, R. J. Warburton, K. Karrai, T. Amand, B. D. Gerardot, P. M. Petroff, and J. M. Garcia, Phys. Rev. B **69**, 035304 (2004).
[28] A. Vasanelli, R. Ferreira, and G. Bastard, Phys. Rev. Lett. **89**, 216804 (2002).